Bidirectional Ecosystem−Atmosphere Fluxes of Volatile Organic Compounds Across the Mass Spectrum: How Many Matter?

Dylan B. Millet,*,[†] Hariprasad D. Alwe,[†] Xin Chen,[†] Malte Julian Deventer,[†] Timothy J. Griffis,[†] Rupert Holzinger,[‡] Steven B. Bertman,[§] Pamela S. Rickly,[∥] Philip S. Stevens,[∥] Thierry Léonardis,[⊥] Nadine Locoge,[⊥] Sébastien Dusanter,[⊥] Geoffrey S. Tyndall,[¶] Sergio L. Alvarez,[○] Matthew H. Erickson,[○] and James H. Flynn[○]

[†]University of Minnesota, Saint Paul, Minnesota 55108, United States
[‡]Utrecht University, Utrecht 3584 CC, The Netherlands
[§]Western Michigan University, Kalamazoo, Michigan 49008, United States
[∥]Indiana University, Bloomington, Indiana 47405, United States
[⊥]IMT Lille Douai, Univ. Lille, SAGE - Département Sciences de l'Atmosphère et Génie de l'Environnement, 59000 Lille, France
[¶]National Center for Atmospheric Research, Boulder, Colorado 80305, United States
[○]University of Houston, Houston, Texas 77004, United States

S Supporting Information

ABSTRACT: Terrestrial ecosystems are simultaneously the largest source and a major sink of volatile organic compounds (VOCs) to the global atmosphere, and these two-way fluxes are an important source of uncertainty in current models. Here, we apply high-resolution mass spectrometry (proton transfer reaction-quadrupole interface time-of-flight; PTR-QiTOF) to measure ecosystem−atmosphere VOC fluxes across the entire detected mass range (m/z 0−335) over a mixed temperate forest and use the results to test how well a state-of-science chemical transport model (GEOS-Chem CTM) is able to represent the observed reactive carbon exchange. We show that ambient humidity fluctuations can give rise to spurious VOC fluxes with PTR-based techniques and present a method to screen for such effects. After doing so, 377 of the 636 detected ions exhibited detectable gross fluxes during the study, implying a large number of species with active ecosystem−atmosphere exchange. We introduce the reactivity flux as a measure of how Earth−atmosphere fluxes influence ambient OH reactivity and show that the upward total VOC ($\sum$VOC) carbon and reactivity fluxes are carried by a far smaller number of species than the downward fluxes. The model underpredicts the $\sum$VOC carbon and reactivity fluxes by 40−60% on average. However, the observed net fluxes are dominated (90% on a carbon basis, 95% on a reactivity basis) by known VOCs explicitly included in the CTM. As a result, the largest CTM uncertainties in simulating VOC carbon and reactivity exchange for this environment are associated with known rather than unrepresented species. This conclusion pertains to the set of species detectable by PTR-TOF techniques, which likely represents the majority in terms of carbon mass and OH reactivity, but not necessarily in terms of aerosol formation potential. In the case of oxygenated VOCs, the model severely underpredicts the gross fluxes and the net exchange. Here, unrepresented VOCs play a larger role, accounting for ∼30% of the carbon flux and ∼50% of the reactivity flux. The resulting CTM biases, however, are still smaller than those that arise from uncertainties for known and represented compounds.

KEYWORDS: *volatile organic compounds, eddy covariance, flux, emissions, deposition, chemical transport model, reactivity*
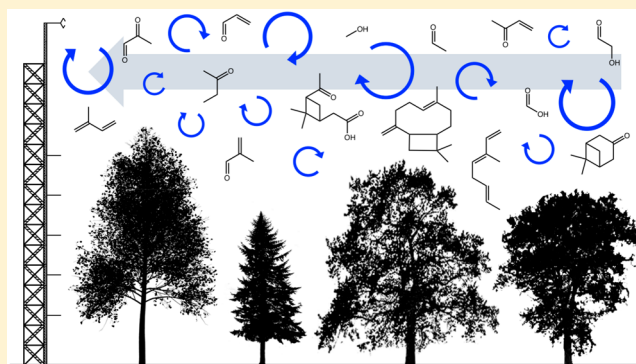
1. INTRODUCTION

Terrestrial ecosystems are by far the largest source of reduced carbon to the atmosphere, with global biogenic emissions of volatile organic compounds (VOCs) thought to exceed 1000 Tg/yr.[1] This exceeds the global flux of methane (∼550 Tg/yr[2]) plus all anthropogenic VOCs combined (∼200 Tg/

yr[3]). Terrestrial plants are also a major VOC sink: global dry deposition of VOCs is estimated at more than 200 Tg/yr,[4] with a large fraction of that going into land ecosystems. This two-way VOC flux is therefore one of the primary levers controlling the chemical properties of Earth's atmosphere; it is also a key source of uncertainty in current chemical transport models (CTMs). One component of that uncertainty is the question of missing or unmodeled VOCs and their potential importance for atmospheric chemistry.

There is known to be a large number of individual VOCs present in the atmosphere. For example, more than 500 ambient VOCs have been identified by 2-dimensional gas chromatography in urban[5] as well remote[6] locations. Park et al.[7] likewise observed approximately 500 ions with detectable land–atmosphere fluxes over a California orange orchard and concluded that there is a large number of reactive VOCs that are not properly represented in current air quality and climate models. In all, Goldstein and Galbally[8] estimated that 10^4–10^5 organic species have been observed in the atmosphere and that this may represent just a small fraction of those actually present. By contrast, current CTMs typically include at most 30–45 VOC tracers (some of which are lumped and surrogates for multiple species). While near-explicit chemical schemes (i.e., the Master Chemical Mechanism; http://mcm.leeds.ac.uk/MCM) are available, they are not tractable to include in their entirety in 3D CTMs for large-scale or long-term simulations. This raises the question of how well our current CTMs, with their necessarily simplified VOC representation, are able to capture the ensemble behavior exhibited by the far larger suite of ambient species.

In this paper, we describe VOC flux measurements performed over a mixed deciduous–coniferous forest by eddy covariance and high-resolution mass spectrometry (proton-transfer reaction-quadrupole interface time-of-flight mass spectrometry; PTR-QiTOF). The data provide a direct measure of the net ecosystem–atmosphere VOC flux across the entire detected mass range, and we use these results to test: (i) how well a state-of-science CTM (GEOS-Chem) is able to capture the land–atmosphere reactive carbon flux in this type of forested environment and (ii) the importance of unrepresented (i.e., detected but unmodeled) VOCs. The analysis by its nature is limited to those VOCs that can be measured by the PTR-TOF technique. However, the most comprehensive characterization of atmospheric reactive carbon to date (with measurements spanning C_1–C_{19} and 19 orders of magnitude in volatility) showed in a forest environment that species observed by PTR-TOF-MS accounted for the majority of all detected VOC–carbon and hydroxyl radical (OH) reactivity.[9] The same did not hold for organic aerosol formation potential. We therefore frame this paper in terms of the gas-phase impacts of the observed VOC fluxes. As part of the analysis, we present a new perspective on the connection between VOC fluxes and ambient OH reactivity: that of the reactivity flux, which is related to the time-rate-of-change in OH reactivity due to surface-atmosphere VOC exchange.

2. METHODS

2.1. Field Site. The AMOS (Atmospheric Measurements of Oxidants in Summer) study took place during July 2016 at the PROPHET (Program for Research on Oxidants: Photochemistry, Emissions, Transport) tower (45.559 °N, 84.715 °W, 232 m elevation) at the University of Michigan Biological Station near the north end of the lower peninsula of Michigan,

United States. The surrounding mixed deciduous/coniferous forest is in a late transitional stage following clear-cutting in the late 1800s. The ~23 m forest includes bigtooth aspen, quaking aspen, and paper birch (upper canopy); white pine, red maple, and American beech (lower canopy); and red oak (both upper and lower canopy).[10,11] There are minimal sources of pollution in the surrounding area (median daytime [10:00−20:00 EDT] NO during PROPHET-AMOS was 23 ppt). There has been a long history of atmospheric measurements at the tower since its construction in 1997,[12] including studies focusing on individual VOCs or classes of VOCs such as isoprene and monoterpenes,[13−21] sesquiterpenes,[22] oxygenated VOCs,[16,23−25] and organic nitrates.[26,27]

A wide suite of chemical measurements was made during PROPHET-AMOS at the 31 m PROPHET walk-up tower and attached triangular tower that extends to 34 m. Chemical observations included VOCs, OH, HO₂, and $\sum RO_2$; OH reactivity; NO, NO_2, NO_3, NO_y, HONO, N_2O, O_3, CO, and SO_2; and a range of aerosol properties. Nonchemical observations included photolysis rates, meteorological parameters, and turbulence at 6 heights (34, 31, 29, 21, 13, and 5 m) by sonic anemometry. Additional trace gas and meteorological measurements were made at the 46 m US-UMB Ameriflux tower (45.560 °N, 84.714 °W, 234 m elevation), ~130 m northeast of the PROPHET tower. Data sets used in the present study are described in detail below.

2.2. VOC Measurements. *2.2.1. Sampling Configuration.* VOC measurements by PTR-QiTOF (Ionicon Analytik, GmbH) were made from 6 sampling heights on the PROPHET tower: 34, 21, 17, 13, 9, and 5 m. The measurement sequence cycled hourly between these inlets using a custom-built automated sampling manifold with 30 min per hour spent sampling from the 34 m inlet and 5 min per hour from each of the other inlets. The remaining 5 min of each hour was used to perform a measurement blank as described below.

The 34 m inlet was installed at the end of a 1.8 m sampling boom extending northwest from the top of the triangular tower. The remaining inlets were installed on 0.9 m sampling booms extending westward from the walkup tower. All inlet lines were 0.5″ OD/0.375″ ID perfluoroalkoxy (PFA) polymer, identical in length, wrapped, and heated to ~50 °C to minimize VOC−wall interactions and avoid water condensation inside the air-conditioned laboratory. Each sampling inlet was continuously flushed even when offline during the hourly sampling sequence. In addition to the inlet lines themselves, all wetted sampling surfaces (including valves) were composed of PFA. Sampling lines were each equipped with an inline filter holder containing a 47 mm diameter 10 μm polytetrafluoroethylene (PTFE) filter installed that was replaced every ~2−3 days. Two rotary vane pumps (1023 Series, Gast Manufacturing Inc.) were used for sampling, with one dedicated to the 34 m eddy covariance inlet and the second used for the other 5 inlets. Flow rates were approximately 40 standard L/min (SLM) for the 34 m inlet and 5−10 SLM for the others, corresponding to inlet residence times of approximately 5 and 30 s, respectively.

2.2.2. Instrument Operation. Measurement blanks (5 min) were performed hourly using zero air generated by passing ambient air from the 34 m sampling inlet through a Pt-bead catalyst (3.2 mm diameter; Shimadzu Corp.) heated to 400 °C. Each hourly blank was averaged (excluding 30 s buffers at the start and end of the 5 min window), and ion background

values for each 10 Hz time point were then obtained by interpolating these hourly blanks based on a cubic smoothing spline. Calibration curves (4-point) were performed daily for a set of 27 VOCs (Table S1) by dynamic dilution (to approximately ambient levels) of certified, gravimetrically prepared, ppm-level compressed standards (prepared in June 2015 by Apel-Reimer Environmental Inc.) into zero air generated as above. A linear fit of the resulting (daily) slopes was then employed to derive time-resolved calibration factors. On the basis of the supplier's past experience for the compounds in Table S1 and their concentrations in the compressed standards, the certified concentrations are expected to be stable for significantly more than one year (a possible exception is hydroxyacetone).

Several additional VOCs were postcalibrated based on laboratory measurements after the campaign and response ratios relative to compounds calibrated in-field. Calibration factors for the other m/z values were then estimated based on the range of sensitivities observed for the calibrated subset. Specifically, the median, highest, and lowest (excluding alcohols) observed sensitivities across all calibrated compounds were used respectively as best estimate, upper, and lower confidence limit for the noncalibrated set. These response factors varied by >4× between the low-sensitivity (propene), median (furan), and high-sensitivity (acetonitrile) assumptions.

Instrumental settings were selected for optimal combination of high sensitivity, high mass resolution, and low humidity-dependence. The PTR drift tube was held at 3.8 hPa and 80 °C with E/N = 132 Td. The time-of-flight analyzer was operated over an m/z range of 0−335 (extraction period 32.5 μs), with the mass axis calibrated continuously via addition of a diiodobenzene internal standard. For acetone, this led to a sensitivity of up to ∼1000 cps/ppb and mass resolution ($\Delta m/m$) of ∼3500.

Peak fitting and integration was performed with the PTR-MS VIEWER 3.2.5 postprocessing software. A custom peak table was developed for PROPHET-AMOS that included 636 detected peaks from m/z 26 to 335. Molecular formulas were assigned to the detected peaks based on the workflow shown in Figure S1 and with the aid of the PTRwid database.[28] All subsequent data processing was performed using a custom set of R (www.r-project.org) routines (available from the authors upon request).

2.2.3. Signal Normalization and Humidity Correction. Standard practice for ambient PTR-based measurements has been to normalize the analyte ion signals by that of the H_3O^+ reagent ion (generally the $H_3(^{18}O)^+$ signal is used; m/z 21.022). Any additional humidity-dependence for the compound and instrumental settings at hand can be accounted for based on the $H_3O^+(H_2O)/H_3O^+$ ratio, which serves as a reliable proxy for the relative humidity (RH) of the sampled airstream.[29,30] Such humidity dependencies can arise from a number of processes such as (i) analyte reactions with $H_3O^+(H_2O)$ clusters; (ii) water-driven fragmentation of analyte-H^+ product ions; (iii) reverse reaction of analyte-H^+ product ions with H_2O; (iv) altered transmission efficiency for H_3O^+ (subsequently used for product ion normalization) between the drift tube and the mass spectrometer;[31] or, as shall be seen here, (iv) changes to the relative abundance of ion source impurities such as O_2^+ and NO^+ that can also react with analyte VOCs. While O_2^+ and NO^+ reactions (e.g., via charge transfer, hydride abstraction, hydroxide abstraction, or

clustering) tend to produce different product ions than the corresponding H_3O^+ reactions, fluctuations in their abundance will nonetheless lead to fluctuating ion signals that could be misinterpreted as VOC fluxes at those masses. Air density fluctuations due to humidity changes (the so-called Webb−Pearman−Leuning effect[32]) can also contribute to the overall humidity dependence; unlike the other effects above, here, the sign of the effect would be the same across all VOCs.

Humidity dependence may become especially important for flux measurements over wet or vegetated surfaces because evapotranspiration drives an eddy correlation between ambient humidity and the vertical wind fluctuations. Those humidity fluctuations will then imprint a corresponding eddy correlation on the measured signal for any humidity-sensitive VOC, yielding an apparent flux when in reality there may be none. For a given humidity sensitivity, such effects will be greater for compounds with high concentration-to-flux ratios: the magnitude of the resulting fluctuations may then be large relative to those from actual surface-atmosphere fluxes.

In this paper, we explicitly examine how humidity fluctuations can affect eddy flux measurements of VOCs by PTR-based techniques. First, we evaluate a range of laboratory-derived correction schemes in terms of their ability to remove any humidity correlation from the field-based calibration responses. Later (Section 3.1), we employ the diiodobenzene internal standard (used for mass axis calibration) to test for any residual humidity effects on inferred fluxes. Therein, we propose a new method for estimating a flux detection limit for humidity-dependent measurements.

Humidity sensitivities for all calibrated VOCs were characterized in the laboratory postcampaign. Five alternate strategies were then employed for humidity correction and normalization of the field data set: (1) normalization to the H_3O^+ reagent ion, with no further humidity correction (approach designated as m21); (2) humidity correction using the X_R approach of de Gouw et al.,[33] which assumes that reaction rate differences for VOCs + $H_3O^+(H_2O)$ versus VOCs + H_3O^+ are the predominant cause of humidity effects (xr21); (3) normalization to H_3O^+ and subsequent humidity correction based on a log−linear fit of the calibration response to $H_3O^+(H_2O)/H_3O^+$ (log21); (4) same as 3, but using a log−log fit of the calibration slopes to $H_3O^+(H_2O)/H_3O^+$ (loglog21); and (5) no normalization (none).

The m21, xr21, log21, and loglog21 approaches yield comparable field calibration fit quality (e.g., R^2 = 0.94−0.96 for methanol when treating all calibration curves as a single statistical ensemble). The no-normalization approach yields much greater variation in calibration response (corresponding R^2 = 0.59) because reagent ion abundance and mass-independent sensitivity fluctuations are then no longer inherently accounted for. The individual (daily) field calibration slopes derived with the xr21, log21, and loglog21 humidity normalizations show less correlation with $H_3O^+(H_2O)/H_3O^+$ (and thus RH) than simple reagent ion normalization (m21 approach). For example, the RH correlation for the ethanol calibration slope drops from R^2 = 0.22 for m21 to R^2 = 0.03 for log21. Field calibrations for the no-normalization data set correlate strongly with H_3O^+ and $H_3O^+(H_2O)$ (median R^2 = 0.8 and 0.5, respectively), but not with their ratio (median R^2 < 0.01), implicating instrumental factors and not ambient humidity as the dominant cause of fluctuating sensitivity in this case. Below, we use the log21 treatment as default and further evaluate the effect of humidity

on measured fluxes based on eddy correlation analysis of our internal standard (Section 3.1).

2.3. Other Measurements. Turbulence measurements used here were performed using a 3D sonic anemometer (CSAT 3B, Campbell Scientific Inc.) collocated with (0.1 m above) the 34 m VOC sampling inlet and oriented into the prevailing wind. Photosynthetic photon flux densities were measured at the US-UMB tower (46 m height) using a BF5 Sunshine Sensor (Delta-T Devices Ltd.). Measurements of temperature and RH were collected with a Vaisala HMP-60 in a 6-plate radiation shield at the top of the PROPHET tower, and with an RM Young 41382 sensor and 41003 radiation shield at 6 m elevation (below-canopy).

Other chemical measurements used here include total OH reactivity and additional trace gas measurements used with the PTR-QiTOF data to compute speciated OH reactivity for comparison with the observed total. Total OH reactivity was measured above the forest canopy using an atmospheric pressure turbulent flow tube reactor.[34] In this technique, OH radicals are produced in a movable injector by photolysis of water vapor and mixed with ambient air inside a 75 cm long (5 cm ID) glass flow tube. Ambient air is brought into the reactor through an 8 cm ID hose constructed of PFA polymer film, with the inlet placed approximately 25 m above ground level. The resulting OH decays (reflecting the reactivity of ambient air) were measured as a function of reaction time by laser-induced fluorescence. The instrument was calibrated by measuring reactivities for a set of compounds with well-known rate constants.[34]

An online gas chromatograph equipped with two columns and two flame ionization detectors was used to monitor 58 nonmethane hydrocarbons (24 alkanes, 14 alkenes, 16 aromatics, 3 alkynes and isoprene) from 8 to 24 July as described in Badol et al.[35] Ambient air was sampled through a Nafion dryer and a thermodesorption unit (ATD 400; PerkinElmer Inc.) containing a VOC-trap held at −30 °C and filled with Carbosieve SIII and Carbopack B. The sample was then thermodesorbed into the two columns (PLOT alumina and CP-Sil 5 CB) to separate C_2–C_6 and C_6–C_{12} compounds. Detection limits of 10–40 ppt were achieved at a time resolution of 90 min.

Ozone (O_3), carbon monoxide (CO), and sulfur dioxide (SO_2) were measured using a common inlet at 6 m. Ozone was measured using a Model 205 (2B Technologies, Inc.) dual-beam UV absorption instrument. CO was measured by off-axis integrated cavity output spectroscopy (CO-23R; Los Gatos Research, Inc.), and SO_2 by pulsed fluorescence (43i-TLE; Thermo Fisher Scientific, Inc.) with hourly baseline evaluations using a carbonate impregnated filter.[36]

NO and NO_x (NO + NO_2) mixing ratios were measured by chemiluminescence using the instrumental design of Ridley and Grahek.[37] A flow of 1 SLM ambient air was drawn from the community manifold into a photolysis cell, which was held at 400 Torr and surrounded by a bank of LEDs for photolyzing NO_2. After passing through a flow controller, the air flow entered the instrument, where it was humidified and entered the reaction vessel. There, it was mixed with a flow of ~8% O_3 in O_2, and the resulting NO–O_3 chemiluminescence was measured using a cooled photomultiplier. The LED power was cycled every 2 min, leading to sequential measurements of NO and [NO + NO_2]. The instrument was zeroed for 10 min hourly with independent NO and NO_2 calibrations performed every 6 h.

2.4. Flux Calculation. Net ecosystem fluxes and exchange velocities were determined for all ion peaks based on the covariance (at 10 Hz) between the (rotated) vertical wind fluctuations (w') and the calibrated, blank-, and humidity-corrected concentration fluctuations (c'). The lag time between w' and c' (associated with inlet-to-detector VOC transit times and instrumental response) was determined by maximizing their correlation for each flux window and compound with requirements for a physically realistic time range (0–10 s) and identifiable maximum ($R > 0.1$). For cases failing one or both of the above criteria, the lag time was interpolated from the time series of valid isoprene lags over the campaign. Isoprene had the largest measured fluxes of any detected species with clearly defined lags: those meeting the above criteria had a median of 5.3 s and varied little over the course of the campaign (0.1–0.9 quantiles: 4.6–6.2 s).

Quality control for the derived fluxes was performed according to standard best practices. This included raw data despiking,[38] removal of nonphysical values, and testing for developed turbulent conditions ($u*$ filtering). We tested for nonstationarity by applying the covariance test recommended by Foken and Wichura[39] to the isoprene fluxes. Time-averaged results were not appreciably different with or without this filter, and it is therefore not used in what follows. Canopy VOC storage terms were calculated each hour from the interpolated in-canopy profile measurements. Storage changes from 1 h to the next were then added to the above-canopy eddy covariance measurements to derive the overall net VOC fluxes. Figure S2 compares the above-canopy versus canopy storage fluxes for some example VOCs and shows that for species with large fluxes, the storage term is only a small fraction of the total. For other species (e.g., MVK+MACR in Figure S2), storage changes can be significant, particularly during morning and evening transitions.

Spectral analysis was performed to evaluate the measured fluxes for a selection of VOCs with varying functionality and spanning the sampled mass range (Figures S3 and S4). In general, the cospectra exhibit behavior consistent with that for sensible heat ($w'T'$) and show that the instrument response time and flux averaging interval are sufficient to quantify fluxes at this site. We estimated the amount of flux attenuation due to factors such as inlet dampening, instrument response, and sensor separation by fitting a single transfer function and attenuation time constant[40] to each weighted, normalized cospectrum. The fractional flux loss for each of these VOCs was then quantified by applying the fitted transfer function to the observed $w'T'$ cospectrum. Results ranged from <2% flux loss for isoprene and monoterpenes; to <5% loss for methanol, acetaldehyde, acetone, and acrolein; to <10% loss for formic acid and hydroxyacetone; to <25% loss for sesquiterpenes and monoterpene oxidation products. Because these are smaller than other sources of analysis uncertainty, no attenuation correction was made to the derived VOC fluxes.

Flux uncertainties were estimated from the $w'c'$ covariance across a range of unrealistic lag times. Fluxes were considered to be above the eddy detection limit if they exceeded the envelope of values seen for lag times of 40–60 s: specifically, if $F > \varepsilon_\mu + \varepsilon_\sigma$ (for positive fluxes) or $F < \varepsilon_\mu - \varepsilon_\sigma$ (negative fluxes), where ε_μ and ε_σ are the mean and standard deviation of the spurious flux values.

2.5. GEOS-Chem Simulation. A high-resolution GEOS-Chem (v10-01; www.geos-chem.org) simulation with updated treatment of VOCs was performed for the PROPHET-AMOS
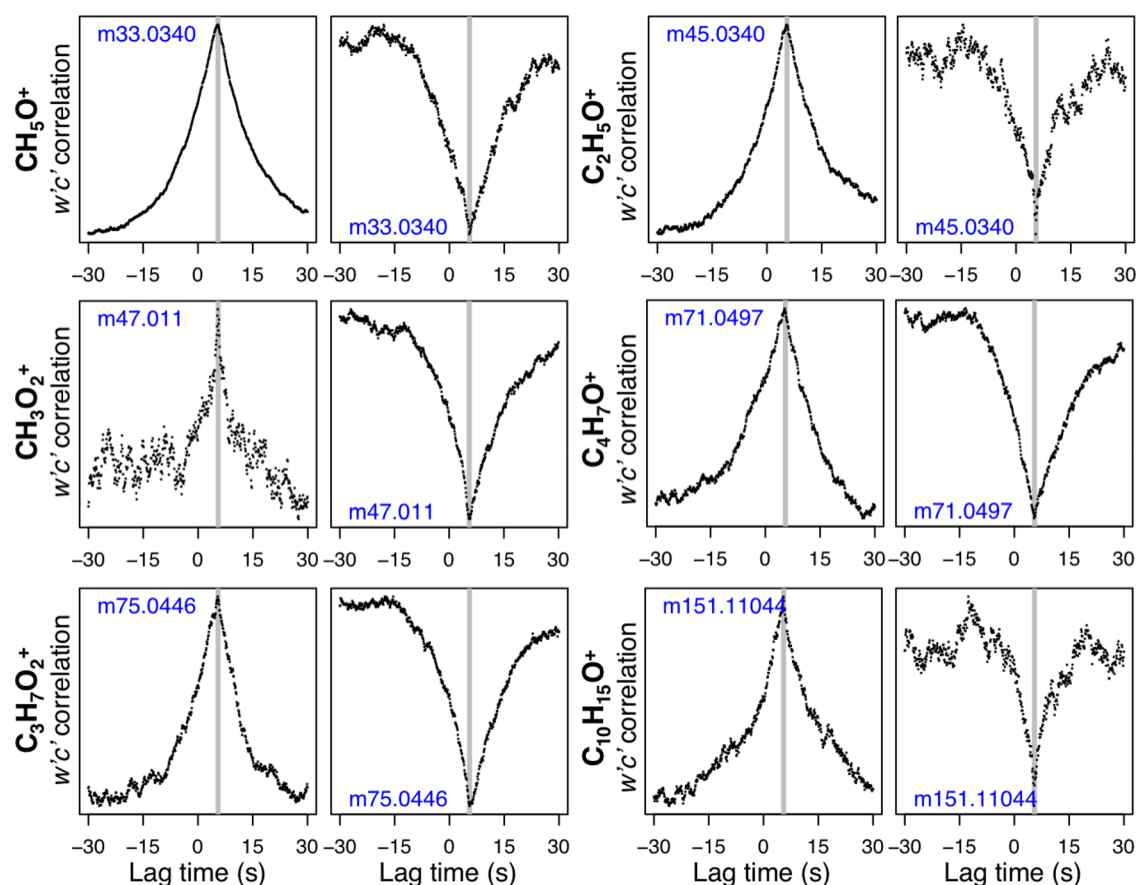
Figure 1. Normalized $w'c'$ correlation as a function of time lag for methanol (CH_5O^+), acetaldehyde ($C_2H_5O^+$), formic acid ($CH_3O_2^+$), methylvinyl ketone + methacrolein ($C_4H_7O^+$), hydroxyacetone ($C_3H_8O_2^+$), and a likely monoterpene oxidation product ($C_{10}H_{15}O^+$, e.g. pinonaldehyde fragment). Values shown represent the ensemble mean lag-correlations for all upward (left columns) and downward (right columns) fluxes meeting the $u*$ and detection thresholds described in-text.

study period. The model uses assimilated meteorological data (Goddard Earth Observation System Forward Processing product; GEOS-FP) from the NASA Global Modeling and Assimilation Office (GMAO), which have native horizontal resolution of $0.25° \times 0.3125°$ with 72 vertical layers. The GEOS-FP fields have 3-h temporal resolution for 3-D meteorological parameters and 1-h resolution for surface quantities and mixing depths. Simulations here use the TPCORE advection algorithm,[41] convective mass fluxes from the GEOS-FP archive,[42] nonlocal boundary layer mixing as described by Lin and McElroy,[43] and wet and dry deposition as described by Amos et al.[44] and Wang et al.[45] Initial simulations revealed a ~0.5−1 K low bias in the GEOS-FP temperature fields relative to the PROPHET-AMOS observations, with a corresponding bias in the simulated biogenic VOC emissions. For the simulations used here, we correct this bias (for the purposes of biogenic emissions only) based on a linear regression between the modeled and measured temperatures.

We use here the nested capability developed by Kim et al.[46] to perform continental-scale simulations over North America at the native $0.25° \times 0.3125°$ resolution of the GEOS-FP data, with dynamic boundary conditions from a global model run at $2° \times 2.5°$. The nested simulation was configured with timesteps of 5 min (transport/convection) and 10 min (emissions/chemistry), with the global simulation using (respectively) 15 and 30 min.[47]

The GEOS-Chem chemical mechanism features comprehensive HO_x−NO_x−VOC−ozone−BrO_x chemistry coupled to aerosols and incorporates the most recent JPL/IUPAC recommendations. Photolysis frequencies are calculated using the Fast-JX algorithms developed by Bian and Prather.[48,49] Isoprene chemistry is as described by Mao et al.[50] In addition, we incorporate here a suite of recent updates pertaining to VOCs, including carboxylic acids and their precursors,[51,52] dicarbonyls and their precursors,[53−55] alcohols and aldehydes,[56−59] and Criegee intermediates.[51] VOCs represented in the simulations presented here include 11 hydrocarbons and 31 oxygenated VOCs (including 8 organic nitrates). Hydrocarbons include isoprene, a lumped monoterpene, ethane, propane, lumped $\geq C_4$ alkanes, ethene, lumped $\geq C_3$ alkenes, acetylene, benzene, toluene, and C_8 aromatics. Oxygenated VOCs include methanol, ethanol, methyl butenol, formaldehyde, acetaldehyde, vinyl alcohol, lumped $\geq C_3$ aldehydes, acetone, lumped $\geq C_4$ ketones, methyl vinyl ketone (MVK), methacrolein (MACR), glycoaldehyde, hydroxyacetone, formic acid, acetic acid, peroxyacetic acid, isoprene-derived C_5 acids, other $\geq C_3$ organic acids, glyoxal, methyl glyoxal, methyl hydroperoxide, isoprene hydroxyl hydroperoxides, and isoprene epoxides. Organic nitrates include propanone nitrate, isoprene hydroxynitrate, MVK/MACR nitrates, $\geq C_4$ alkylnitrates, methyl peroxy nitrate, peroxyacetylnitrate, peroxypropionylnitrate, and peroxymethacryloyl nitrate.

Emissions in GEOS-Chem employ the HEMCO module developed by Keller et al.[60] Biogenic VOC emissions from terrestrial plants are computed online in GEOS-Chem using the Model of Emissions of Gases and Aerosols from Nature
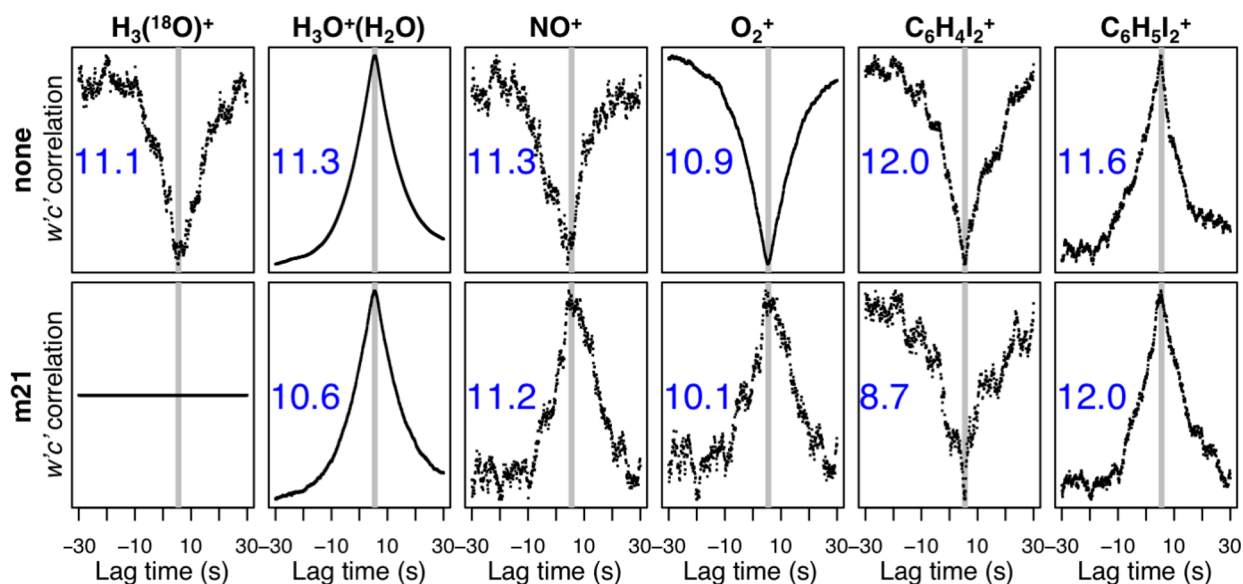
Figure 2. Apparent $w'c'$ correlation (normalized) as a function of time lag for the reagent ion ($H_3(^{18}O)^+$), several contaminant ions generated in the PTR instrument ($H_3O^+(H_2O)$, NO^+, O_2^+), and for two peaks associated with the diiodobenzene internal standard ($C_6H_4I_2^+$, $C_6H_5I_2^+$). Top row shows raw ion signals, and bottom row shows signals normalized to $H_3(^{18}O)^+$. Numbers inset indicate the signal-to-noise (ratio of peak correlation to the mean + standard deviation of correlations at large lag times).

version 2.1 (MEGAN v2.1).[1] Biogenic VOC emissions predicted by MEGAN and similar models can be highly sensitive to the choice of input data sets (e.g., leaf area index, meteorology, vegetation cover) and canopy parametrization; here, we use the standard GEOS-Chem implementation described by Hu et al.[61] Specifically, the MEGAN emissions are derived using monthly mean leaf area indices[62] from the Moderate Resolution Imaging Spectroradiometer (MODIS), plant functional type distributions[63] from version 4 of the Community Land Model (CLM), and the Parameterized Canopy Environment Emission Activity (PCEEA) algorithms.[64] Relevant meteorological variables (e.g., direct and diffuse photosynthetically active radiation; air temperature) are taken from the GEOS-FP fields used to drive GEOS-Chem.

Global anthropogenic VOC emissions are taken from the Interpolated ACCMIP-RCP 8.5 data set[65−67] for the year of our simulation, while global anthropogenic $NO_x/CO/SO_2$ emissions are from EDGAR v4.2.[68] NO_x emissions from natural soil, fertilizer, and deposited N pools are estimated following Hudman et al.[69] Over North America, anthropogenic emissions are overwritten by the United States Environmental Protection Agency National Emission Inventory for 2011[70,71] with annual scale factors to account for subsequent changes. Modeled air−sea VOC fluxes are adapted from Fischer et al.[72] Other emissions are kept as default in GEOS-Chem.[73−78]

3. RESULTS AND DISCUSSION

We find that the majority of the 636 ions detected at PROPHET-AMOS exhibit bidirectional exchange, with periods of both upward (canopy emission) and downward (canopy uptake) fluxes. Figure 1 shows $w'c'$ lag-correlation plots for some example VOCs, demonstrating two-way fluxes for compounds with purely primary (direct emission), purely secondary (photochemical production), and both primary + secondary sources. Later (Section 3.4), we examine these two-way fluxes in more detail and assess how well they are represented in the GEOS-Chem CTM.

In the following section, we present an approach for testing which measured fluxes exceed the detection limit imposed by the humidity dependence of PTR-based measurements. We then examine the importance of the detected fluxes across the mass spectrum for atmospheric composition.

3.1. Role of Humidity in Biasing PTR-Based Fluxes. For PTR-based and other humidity-sensitive measurements, land−atmosphere water fluxes can cause artifactual fluxes by creating fluctuating instrumental sensitivities that correlate with w'. Figure 2 illustrates this effect, showing $w'c'$ lag-correlation plots analogous to Figure 1, but for three contaminant ions generated in the PTR instrument: $H_3O^+(H_2O)$, NO^+, and O_2^+. We see in each case a correlation with w', suggesting a flux, but in fact reflecting the tendency for these contaminant ions to vary with humidity. Because these three ions, like H_3O^+, react with VOCs, we should expect the distribution of VOC product ions to have some w' correlation, independent of any real VOC fluxes. In the case of NO^+ and O_2^+, we see that the sign of the w' correlation changes when signals are normalized to that of $H_3(^{18}O)^+$. In other words, the standard PTR practice of normalizing VOC ion signals to m/z 21.023 can by itself impart some degree of w' correlation.

While we explicitly account for humidity-dependent sensitivities for our set of calibrated compounds, this is not possible for all of the 636 detected ion peaks, many of which represent unidentified VOCs. We therefore assess here the impact of the above effects on our measured fluxes. To this end, we employ the mass spectral peaks associated with the internal standard (diiodobenzene, $C_6H_4I_2$) used for calibration of the TOF mass axis. These provide a stable signal at a distinctive set of m/z ratios that are unlikely to be affected by detectable forest−atmosphere fluxes of $C_6H_4I_2$. The large negative mass defect imparted by the two iodine atoms, combined with the high internal standard concentrations relative to ambient VOCs in that part of the mass spectrum, also makes any detectable influence from interfering species or fragments unlikely. These masses are thus useful markers for spurious fluxes caused by instrumental factors.

Figure 2 (right 2 columns) shows lag correlations for $C_6H_4I_2^+$ and $C_6H_5I_2^+$, two peaks arising from the $C_6H_4I_2$ standard addition. Here also a significant w' correlation is evident, imparted by humidity-driven fluctuations in instrumental response. Because $C_6H_4I_2$ is added to the instrument at a constant, controlled rate, we should expect all ambient VOC signals to be subject to corresponding, spurious, w' correlations. Also, while $C_6H_5I_2^+$ (from $C_6H_4I_2 + H_3O^+$) has a net positive w' correlation, $C_6H_4I_2^+$ (from $C_6H_4I_2 + O_2^+$) has a net negative correlation. In other words, the sign of the effect (giving apparent positive or negative fluxes) will vary for different ion peaks.

Figure 3 (panels a and b) shows the diel average apparent exchange velocity (v_e; flux divided by number density) for $C_6H_5I_2^+$ over the course of the campaign. Daytime values average $\sim0.05-0.1$ cm/s for the raw ion signals and increase to $\sim0.1-0.2$ cm/s for the H_3O^+-normalized signals. Because the

parent $C_6H_4I_2$ concentrations are in reality close to constant, these apparent exchange velocities can be taken as an inherent flux detection limit based on the humidity dependence of PTR-based measurements. Our approach in the remainder of this paper is thus to categorize observed VOC fluxes as above detection limit if the magnitude of the exchange velocity exceeds the simultaneously observed value for $C_6H_5I_2^+$.

The sign of the $w'c'$ correlation and apparent exchange velocity shown in Figures 2 and 3 indicate a positive humidity dependence for $C_6H_5I_2^+$ under the instrumental settings used here. Further work is needed to define the mechanism driving this behavior. Of most relevance for its use as a flux filter, however, is that the magnitude of the observed $C_6H_5I_2^+$ humidity effect is in-line with what we expect for the suite of ambient VOCs. Specifically, the $C_6H_5I_2^+$ peak area (with m21 normalization) increases 22% on average from the lowest to highest deciles of RH observed during PROPHET-AMOS (based on the $H_3O^+(H_2O)/H_3O^+$ ratio). The corresponding m21 sensitivity changes for the full set of calibrated VOCs have a mean magnitude of 12% and a range of 0−34%. We therefore view our internal standard-based approach as an appropriate (while not overly stringent) screening threshold for identifying physically meaningful fluxes. In theory, one could employ a set of internal standards spanning a range of humidity dependencies to achieve a more thorough characterization.

After setting all below-detection-limit fluxes to zero (based on the above v_e-based screening procedure), the number of valid flux measurements drops by more than half for 74% of the detected ions, and the total carbon flux drops by more than half for 20% of the ions (Figures 3c and d). However, these filtered values are associated with low fluxes. Figure 3d shows, for the ions that could be assigned a molecular formula (see next section), the relative flux change for each ion as a function of its cumulative absolute flux. We see in the figure that the overall, detected VOC−carbon flux at this site is dominated by a limited set of high-emission and high-deposition compounds: as a result, the v_e-based removal of humidity artifacts does not have a significant effect on the total estimated exchange of VOC−carbon. For the same reason, while humidity effects may still induce some bias in those fluxes large enough to pass the v_e-based screening, the resulting effect on the total measured VOC−carbon flux would be negligible.

The degree to which this finding (i.e., that humidity fluctuations have a negligible effect on the total measured VOC−carbon flux) applies also to other PTR-based flux measurements may depend on the instrumental configuration at hand: settings here were specifically optimized to minimize humidity effects. Prior PTR-TOF eddy covariance studies have varied in their approaches for identifying a flux detection limit. For example, Kaser et al.[79] defined an absolute detection limit below which they did not consider fluxes to be distinguishable from advective influences. Here, we focused on humidity effects, and in this case we consider a threshold based on exchange velocity to be more appropriate because the magnitude of the effect will scale with compound concentration. On the other hand, Park et al.[7] employed a time-shifted covariance analysis similar to that used here (Section 2.4) to define an eddy flux detection limit. This type of approach will properly identify flux signals exceeding random instrumental noise but will not necessarily remove any artificial fluxes imposed by humidity sensitive detection. For analyses in which a large number of small-flux compounds are aggregated to arrive at an overall reactive carbon emission or deposition
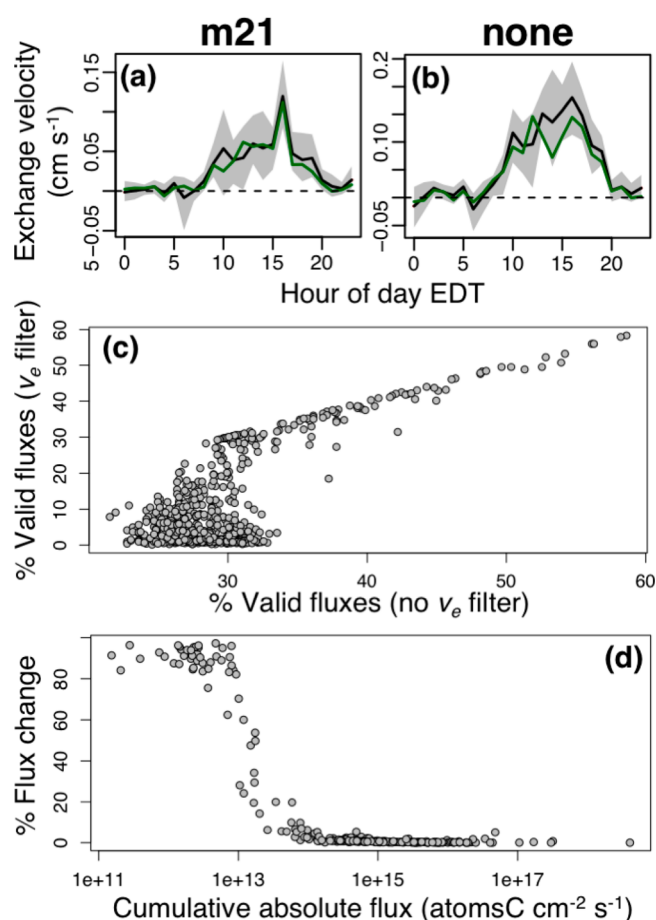

Figure 3. Use of the PTR-QiTOF internal standard to diagnose spurious fluxes due to humidity effects. Panels a and b show the diel average apparent exchange velocity for $C_6H_5I_2^+$, the main product ion for the diiodoenzene internal standard (a: raw ion signals; b: signals normalized to $H_3(^{18}O)^+$). Green lines shows the diel median, while the black lines and shaded regions show the diel mean and associated 95% confidence interval. Panels c and d: effect of imposing a flux detection limit based on the contemporaneous exchange velocity observed for the internal standard. Panel c shows, for each measured m/z ratio, the percent of total flux observations that exceed the detection limit when the v_e threshold is employed versus when it is not. Panel d shows the corresponding relative change in cumulative VOC−carbon flux as a function of the absolute flux.

budget, we recommend explicitly accounting for artifactual humidity-derived fluxes via an internal standard (as here) or other means.

3.2. Most Detected Peaks Exhibit Forest–Atmosphere Fluxes. After screening for humidity artifacts as described above (i.e., setting below-detection-limit fluxes to zero), we find that 180 of the 636 detected peaks have a detectable net forest–atmosphere flux (based on the mean $w'c'$ lag-correlation for the campaign). However, Figure 4a shows
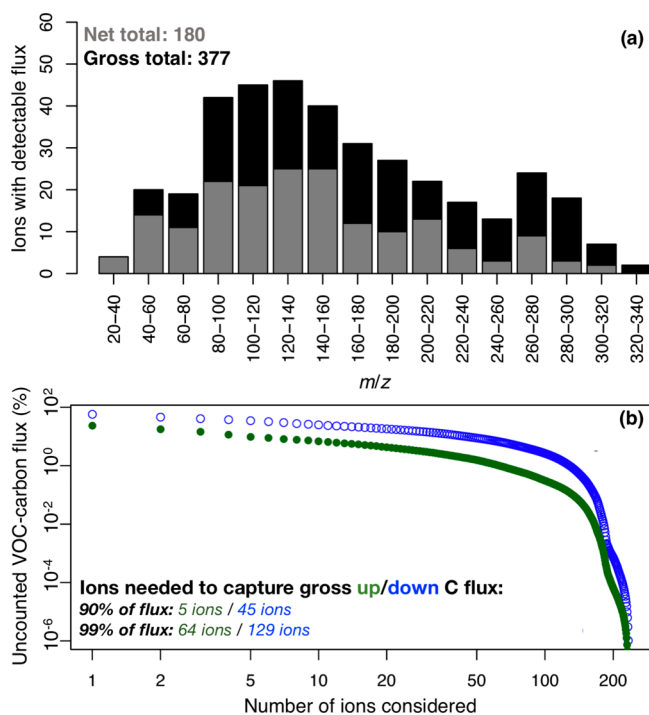

Figure 4. Panel a: number of ions with detectable net (gray) and gross (black) forest–atmosphere fluxes by m/z ratio. Panel b: fraction of the total gross upward (green) and downward (blue) VOC–carbon flux that remains unaccounted for as a function of the number of ions considered.

that more than twice that many (377) have a detectable gross flux (based on the mean absolute $w'c'$ lag-correlation). This is similar to findings from Park et al.[7] over an orange orchard and argues for a very large number of individual VOC species actively exchanging between the forest canopy and the atmosphere. A total of 236 ions could be assigned a molecular formula using the procedure outlined in Figure S1, accounting for >98% of the total molar flux.

What is the importance of all of these species for atmospheric composition? One key metric for this question is the amount of reactive carbon (i.e., VOC–carbon mass) that is being exchanged. Figure 4b shows the fractional VOC–carbon flux that remains unaccounted for as a function of the number of ions considered. Whereas only 5 ions suffice to account for 90% of the gross upward flux, 45 are needed to account for 90% of the gross downward flux. Accounting for 99% of the gross fluxes requires a much larger number of ions: 64 (upward) and 129 (downward).

A few salient points emerge from this analysis. First, we see (at least for this ecosystem) that the cumulative deposition flux of VOC–carbon is carried by a much larger suite of species than is the emission flux. Second, there is a very large number

of species with small individual fluxes, raising a question as to their cumulative importance. Lastly, there are far more ions with active forest–atmosphere exchange than is represented in current chemical transport models, which typically track no more than 30−45 VOCs (some lumped). We therefore need to assess how well the reduced VOC treatment in current CTMs can capture the ensemble flux behavior exhibited by the much larger set of ambient VOCs. In the following section, we examine this issue using the nested GEOS-Chem simulation described in Section 2.5.

3.3. Net Detected VOC–Carbon Flux Is Dominated by Known Compounds. Together, isoprene and monoterpenes account for more than half of the total net VOC–carbon flux detected across the entire mass spectrum, and this is consistent with the model expectation. Observed fluxes for these species are also within the range of what has been observed previously at PROPHET.[14,21] We see in Figure S5 that the GEOS-Chem simulation underestimates isoprene emissions by 30−40% around mid-day, even after correcting the model temperature fields as described in Section 2.5. The decline from the mid-day peak also occurs too soon in the model, so that a much larger underestimate is seen in the afternoon. The daytime monoterpene flux is well-captured by the model (Figure S5). However, model emissions are dramatically too high at night, pointing to an underrepresentation of the light-dependence of monoterpene fluxes. Prior work has found that t-β-ocimene (which is light-dependent) makes up a large fraction of the total monoterpene flux at this site.[21] The simplified monoterpene treatment in the CTM does not capture such effects, which could lead to day−night biases in monoterpene chemistry and the resulting gas- and particle-phase products. Overall, these findings illustrate the persistent uncertainties in representing even the best-studied VOCs in standard CTMs.

Figure 5a compares the diel average total VOC flux ($\sum$VOC, in carbon units) as detected at PROPHET and simulated by GEOS-Chem. The observed fluxes represent the combined effects of surface exchange and vertically dependent chemistry. Because our 34 m sampling height falls within the lowest model layer (which extends to ∼130 m), we place bounds on the model chemical flux using two limiting assumptions: (i) all chemical production and loss is dispersed uniformly through the first model layer, and (ii) all production and loss occurs below the 34 m sampling height. The colored regions in Figure 5 display the resulting ranges for the gross upward, gross downward, and net model fluxes.

We see in Figure 5a that during daytime the total net forest−atmosphere flux of reactive carbon in the model averages only half (or less) of what is observed. However, also plotted in Figure 5a is the portion of the detected flux carried by VOCs that are explicitly represented in the GEOS-Chem CTM, showing that such species make up approximately 90% of the net $\sum$VOC carbon flux. The largest current CTM uncertainties in capturing the net forest−atmosphere $\sum$VOC carbon flux (at least for this type of mixed deciduous-coniferous ecosystem) are thus associated with errors for known compounds already represented in models rather than missing compounds.

This finding clearly applies only to the set of VOCs that are detectable by the PTR-QiTOF technique. However, two lines of argument suggest that this set is likely to account for the majority of the forest−atmosphere VOC−carbon flux. The first comes from a recent study by Hunter et al.,[9] who describes a comprehensive reactive carbon budget across the full expected
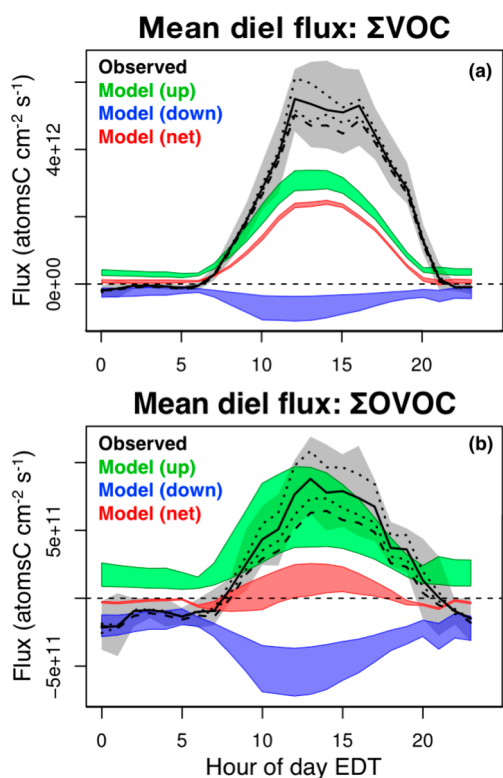
Mean diel flux: ΣVOC

Mean diel flux: ΣOVOC

Figure 5. Mean diel cycle of forest−atmosphere fluxes for the sum of all VOCs ($\sum$VOC, panel a) and the sum of all oxygenated VOCs ($\sum$OVOC, panel b). The black solid line and shaded gray region show the mean observed flux and associated 95% confidence interval. Dotted lines show results using upper and lower sensitivity assumptions for uncalibrated compounds as described in-text. The dashed line shows the mean observed diel cycle for the VOC subset that is explicitly included in the GEOS-Chem CTM. Green, blue, and red regions span upper and lower limits for the model-derived gross upward, gross downward, and net fluxes as described in-text.

ambient range of molecular size, functionality, and volatility (C_1−C_{19}; $c^* = 10^{-8}$ to 10^{10} μg m^{-3}) based on five mass spectrometry techniques at a forested site in Colorado, United States. In that study, species detected by PTR-TOF-MS made up the majority of the total organic carbon mass and OH reactivity. The second argument comes from total OH reactivity measurements at the PROPHET-AMOS study. As discussed in Section 3.5 below, the observed OH reactivity magnitudes can be accounted for (within error) by the suite of species measured by PTR-QiTOF plus other trace gas measurements on-site.

3.4. Oxygenated VOCs Make up the Majority of Species with Detectable Fluxes. Whereas isoprene and monoterpenes make up the majority of the net organic carbon mass flux, the majority of the detected and identified species at PROPHET-AMOS are oxygenated VOCs (OVOCs): of the 236 species with identified molecular formulas, 192 contain at least one oxygen atom (along with carbon).

Figure 6 shows time series of the total measured and modeled OVOC ($\sum$OVOC) fluxes during the campaign. The detected fluxes are bidirectional, exhibiting periods of net canopy emission as well as net canopy uptake. The model $\sum$OVOC fluxes show the same bidirectional character as the observations, but the magnitude of both the upward and downward net fluxes is too small, showing that the model

tends to underestimate both the gross emissions and the gross uptake of OVOCs.

The same pattern is evident in the flux-dependency plots shown at the bottom of Figure 6. The net detected $\sum$OVOC fluxes tend to be upward under sunny and dry (low relative humidity) conditions and downward under darker and wetter conditions. In both situations, the magnitude of the model flux is too small, again demonstrating that the CTM is under-estimating both sides of the bidirectional $\sum$OVOC exchange. Likewise, the mean net daytime $\sum$OVOC flux detected at PROPHET is much larger than the corresponding net model flux (Figure 5b), and in fact is similar to the gross upward flux in the model. These comparisons highlight the need for improved representation of surface-atmosphere OVOC fluxes in current CTMs.

The dashed line in Figure 5b shows the net detected $\sum$OVOC−carbon flux carried by species currently included in the GEOS-Chem CTM, averaging approximately 70% of the total during daytime. Compared to the case for total VOCs, we see here that a significant fraction (∼30%) of the net $\sum$OVOC flux is due to unmodeled compounds. However, the resulting bias in the derived organic carbon flux is still smaller than that from CTM errors for those OVOCs that are modeled (Figure 5b).

3.5. Forest−Atmosphere Reactivity Flux. The carbon-based units employed above quantify the effect of surface fluxes on organic carbon loading in the atmosphere but do not say anything about the chemical impact of those fluxes. One measure of the importance of a given compound for atmospheric chemistry is its OH reactivity ($R_{OH,i} = k_i c_i$ in s^{-1}, with c_i the number density for species i and k_i its reaction rate coefficient with OH), which when summed over all compounds gives the first-order loss rate for ambient OH. We can similarly define the OH reactivity flux for VOC$_i$ as $F_{ROH,i} = k_i F_i$ (cm/s^2) where F_i is that species' surface-atmosphere flux. Because the increment in atmospheric concentration dc_i due to a surface exchange F_i over time interval dt is d$c_i = F_i(\mathrm{d}t/h)$, where h is the atmospheric depth over which the flux manifests, we can write $F_{ROH,i} = hk_i(\mathrm{d}c_i/\mathrm{d}t) = h(\mathrm{d}R_{OH,i}/\mathrm{d}t)$. F_{ROH} thus quantifies the time-derivative of R_{OH} due to surface exchange (scaled to mixing height), providing a direct measure of the influence of surface fluxes on ambient OH reactivity.

To derive F_{ROH} for the PROPHET-AMOS data set, we first assign k_i values from the literature[80] to those VOCs with known or best-guess molecular structures. For VOCs with identified molecular formulas but unknown molecular structures, we estimate k_i using the parametrization proposed by Donahue et al.,[81] with a factor of 3 assumed uncertainty. When tested for the set of detected VOCs with known structures and k_i values, this approach yields a median k_i bias of −9% (median absolute value of the bias is 85%). Figure S6 shows that the ambient R_{OH} calculated in this way and summed over all compounds (including relevant measurements from other instruments on-site) tends to bracket the observed total R_{OH} as measured by laser-induced fluorescence. While this finding differs from that of Di Carlo et al.,[82] who inferred significant missing OH reactivity at this site, that earlier study was based on a far smaller set of VOCs than is detected here (e.g., only 8 OVOC versus the 192 C and O-containing ions detected here).

Figure 7a shows the number of ions needed to account for the cumulative upward and downward VOC reactivity flux detected by PTR-QiTOF during PROPHET-AMOS. The
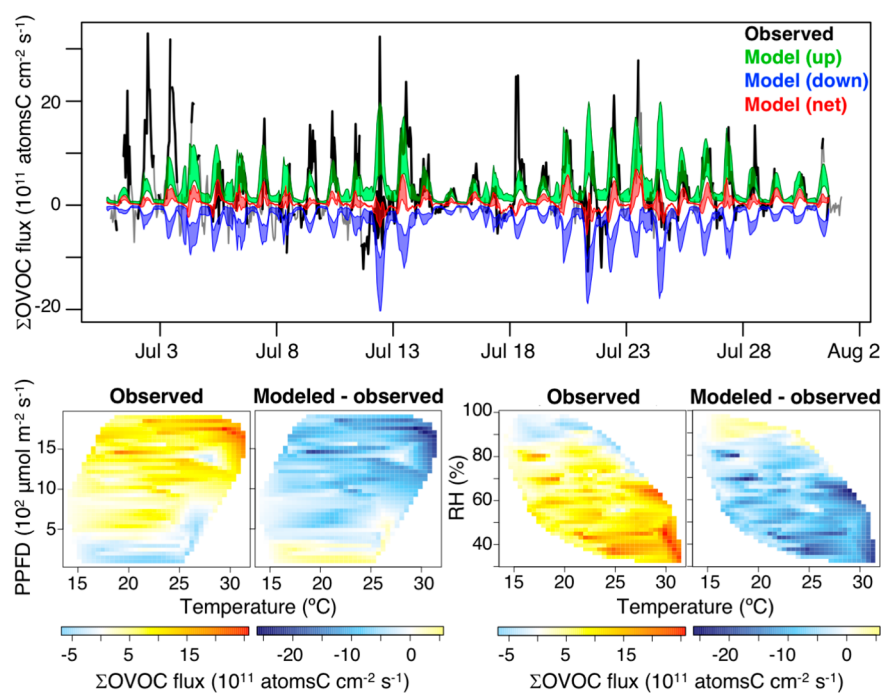
Figure 6. Top panel: time series of total measured (black) versus modeled (colors) oxygenated VOC ($\sum$OVOC) fluxes during PROPHET-AMOS. The gray line shows fluxes that failed to meet the quality control criteria described in-text. Green, blue, and red regions span upper and lower limits for the model-derived gross upward, gross downward, and net fluxes. Bottom row: observed versus modeled dependence of daytime (10:00−17:00 EDT) $\sum$OVOC fluxes on light (photosynthetic photon flux density, PPFD), temperature, and relative humidity (RH).
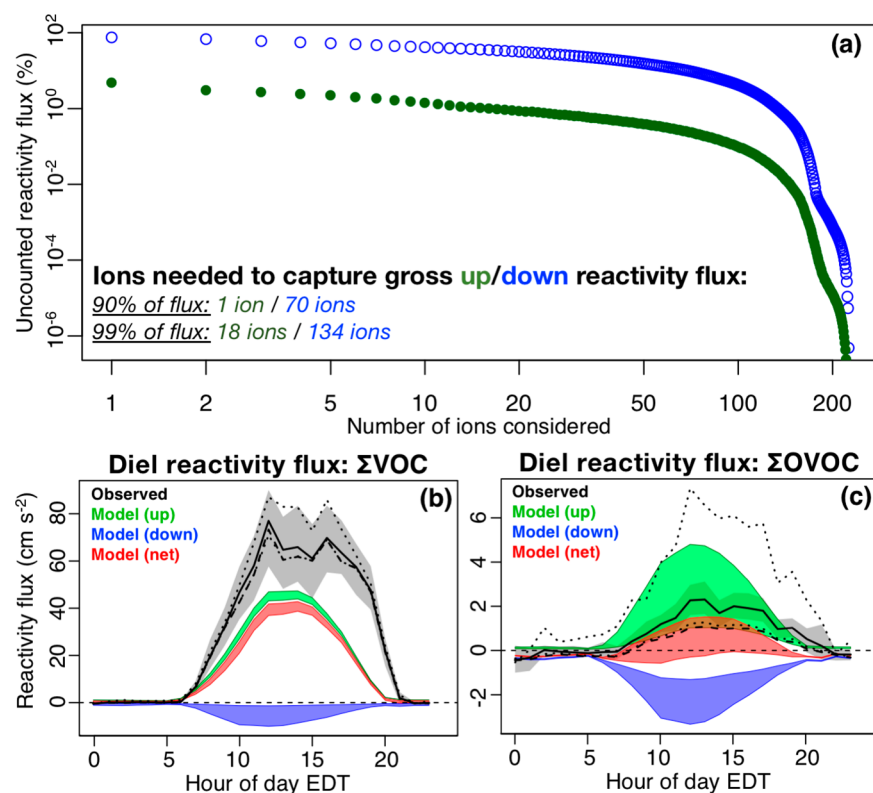

Figure 7. Measured and modeled reactivity flux. Panel a: fraction of the total gross upward (green) and downward (blue) VOC reactivity flux that remains unaccounted for, as a function of the number of ions considered. Panels b and c: mean diel cycle of forest−atmosphere reactivity fluxes for the sum of all VOCs ($\sum$VOC, b) and the sum of all oxygenated VOCs ($\sum$OVOC, c). The black solid line and shaded gray region show the mean observed reactivity flux and associated 95% confidence interval. Dotted lines show results using upper and lower sensitivity assumptions for uncalibrated compounds as described in-text. The dashed line shows the mean observed diel cycle for the VOC subset that is explicitly included in the GEOS-Chem CTM. Green, blue, and red regions span upper and lower limits for the model-derived gross upward, gross downward, and net reactivity fluxes as described in-text.

upward reactivity flux is dominated by a very small number of compounds: for example, a single VOC (isoprene) accounts for 90% of the upward reactivity flux, and only 18 ions are required to capture 99% of the total. This starkly contrasts the downward reactivity flux, which is distributed over a very large number of VOCs: 70 ions are required to capture 90% of the downward reactivity flux, and 134 to capture 99%.

Also shown in Figure 7 is the mean diel cycle of net reactivity flux for all detected and modeled VOCs ($\sum$VOC). We see in the GEOS-Chem simulation an underestimate of the net reactivity flux similar to that found for the VOC−carbon mass flux (Figure 5). However, the net detected VOC reactivity flux is completely dominated by known and modeled compounds (even more than was the case for the VOC−carbon flux), with such compounds accounting for 95% of the total during daytime.

To a large extent, the above finding reflects the importance of isoprene and monoterpenes in this ecosystem; a more challenging model test is to focus on the reactivity flux contributed by other VOCs. Figure 7c shows the diel net reactivity flux for all OVOCs ($\sum$OVOC), which form the majority of detected nonisoprene, nonmonoterpene VOCs. In this case, unmodeled species play a larger role, representing approximately half of the net daytime $\sum$OVOC reactivity flux. However, the missing reactivity flux due to these unknown (or at least unmodeled) detected species still represents a significantly smaller model error than those associated with known and modeled species. For example, we see in Figure 7b that the net modeled $\sum$VOC reactivity flux is ∼20−40 cm/s^2 lower than the observed daytime values (10:00−20:00 EDT mean difference of 30 cm/s^2), whereas the unmodeled OVOC have a maximum daytime reactivity flux of <1.5 cm/s^2.

4. SUMMARY AND IMPLICATIONS

We presented new VOC flux measurements over a transitional deciduous/coniferous forest in Michigan, United States from the PROPHET-AMOS field study. Measurements were performed by high-resolution mass spectrometry (PTR-QiTOF), enabling direct flux measurements by eddy covariance over m/z 0−335. We used these results to test how well a current, state-of-science chemical transport model (GEOS-Chem CTM), with its necessarily simplified treatment of VOCs, is able to represent the two-way forest−atmosphere exchange of reactive organic carbon. While this comparison can pertain only to the set of species measured by the PTR-TOF technique, there is reason to believe from recent field measurements[9] that this set is likely to make up the majority of VOC−carbon and associated OH reactivity.

We first showed that ambient water vapor fluxes can imprint an artificial flux signal on VOCs measured using the PTR technique. The effect arises from humidity-driven changes to the ion chemistry and sensitivity of the instrument and will likewise affect other flux measurements by water-sensitive detection techniques. We developed a new method for identifying VOC fluxes that are below the humidity-caused detection limit using the apparent exchange velocities for an internal standard. After setting these below-detection-limit fluxes to zero, 180 of the 636 detected ions had a significant net flux into or out of the ecosystem, with twice that many having a detectable gross flux. Of those, only 5 ions accounted for 90% of the overall upward VOC−carbon flux, whereas 45 were needed to account for 90% of the overall downward flux.

Deposition fluxes to this ecosystem are thus driven by a much larger number of species than emission fluxes.

We next tested whether the GEOS-Chem CTM was able to reproduce the observed forest−atmosphere VOC flux and found that the diel mean simulated $\sum$VOC flux was only half of what was detected (even after a model temperature correction), while the net and gross $\sum$OVOC exchanges were also severely underestimated. On the other hand, ∼90% of the observed $\sum$VOC flux was carried by known species explicitly included in the CTM (70% for the $\sum$OVOC flux), showing that the largest errors in simulating the overall forest−atmosphere flux of VOC mass were associated with known rather than unknown species. Such model errors for fluxes of known species might be reduced by constraining the factors driving exchange (e.g., leaf area index, plant species distribution, etc.) based on site-specific observations at PROPHET rather than based on the global data sets used in the CTM. Our aim, however, was to assess priority errors for CTMs used for regional and global simulation. Site-specific observations are not available for every single model grid square, and uncertainty in these driving data sets is an important factor in simulating VOC emissions and deposition.

We introduced the reactivity flux as a new metric to describe the impact of surface exchange on ambient OH reactivity. Daytime reactivity fluxes during PROPHET-AMOS were completely dominated (95%) by known and modeled VOCs. This supports earlier work by Kim et al.[16] at the same site, who found no significant contribution from unknown biogenic VOC emission to OH reactivity measured in branch enclosures. We find that a much larger fraction (∼50%) of the OVOC reactivity flux is driven by unrepresented compounds, so that more work is needed to characterize forest−atmosphere exchange for the suite of OVOC contributing to ambient reactivity. However, the OH reactivity bias from omitting these compounds is still smaller than that which arises from the model errors for known VOCs.

The fact that the majority of the VOC flux observed here (both carbon and reactivity-based) is carried by known and modeled species is a positive finding for current CTMs in terms of their potential to adequately represent forest−atmosphere fluxes. As noted, these findings may not extend to the suite of VOCs most important to aerosol formation. Overall, however, the uncertainties that persist for the set of known species clearly highlights the need for better model representation of forest−atmosphere exchange in general.

This research builds on work by Park et al.,[7] who found that VOCs outside the 10 most commonly measured ions accounted for ∼33% of their total observed canopy−atmosphere flux and concluded that there is a large number of additional species that merit study and inclusion in models. Here, ions outside of that traditional set accounted for 14% of the absolute VOC−carbon flux but just 6% of the net flux. The difference likely reflects the ecosystems at hand: an orange orchard in the former case versus a deciduous/coniferous forest in the present case. The PROPHET site could be considered a more straightforward testbed for our models. It is an isoprene-dominated system, with little anthropogenic influence. With Lakes Michigan and Huron to the west and east, one would also expect fewer multigeneration VOC oxidation products than in some other locales. Further research is needed to characterize the full forest−atmosphere VOC flux for other important ecosystems as a function of environmental conditions, stress, and anthropogenic influence.

ASSOCIATED CONTENT

S **Supporting Information**

The Supporting Information is available free of charge on the ACS Publications website at DOI: 10.1021/acsearthspacechem.8b00061.

> Table S1, parameters for compressed VOC standards; Figure S1, workflow for assigning molecular formulas; Figure S2, comparison of above-canopy and canopy storage fluxes; Figures S3 and S4, spectral analysis for example *m/z* ratios; Figure S5, diel cycle of isoprene and monoterpene fluxes; Figure S6, OH reactivity comparison (PDF)

AUTHOR INFORMATION

Corresponding Author
*E-mail: dbm@umn.edu.

ORCID
Dylan B. Millet: 0000-0003-3076-125X
Philip S. Stevens: 0000-0001-9899-4215

Notes
The authors declare no competing financial interest.

ACKNOWLEDGMENTS

REFERENCES

(1) Guenther, A. B.; Jiang, X.; Heald, C. L.; Sakulyanontvittaya, T.; Duhl, T.; Emmons, L. K.; Wang, X. The Model of Emissions of Gases and Aerosols from Nature version 2.1 (MEGAN2.1): an extended and updated framework for modeling biogenic emissions. *Geosci. Model Dev.* **2012**, *5* (6), 1471–1492.

(2) Saunois, M.; Bousquet, P.; Poulter, B.; Peregon, A.; Ciais, P.; Canadell, J. G.; Dlugokencky, E. J.; Etiope, G.; Bastviken, D.; Houweling, S.; et al. The global methane budget 2000–2012. *Earth Syst. Sci. Data* **2016**, *8* (2), 697–751.

(3) Huang, G. L.; Brook, R.; Crippa, M.; Janssens-Maenhout, G.; Schieberle, C.; Dore, C.; Guizzardi, D.; Muntean, M.; Schaaf, E.; Friedrich, R. Speciation of anthropogenic emissions of non-methane volatile organic compounds: a global gridded data set for 1970–2012. *Atmos. Chem. Phys.* **2017**, *17* (12), 7683–7701.

(4) Safieddine, S. A.; Heald, C. L.; Henderson, B. H. The global nonmethane reactive organic carbon budget: A modeling perspective. *Geophys. Res. Lett.* **2017**, *44* (8), 3897–3906.

(5) Lewis, A. C.; Carslaw, N.; Marriott, P. J.; Kinghorn, R. M.; Morrison, P.; Lee, A. L.; Bartle, K. D.; Pilling, M. J. A larger pool of ozone-forming carbon compounds in urban atmospheres. *Nature* **2000**, *405* (6788), 778–781.

(6) Xu, X.; van Stee, L. L. P.; Williams, J.; Beens, J.; Adahchour, M.; Vreuls, R. J. J.; Brinkman, U. A. T.; Lelieveld, J. Comprehensive two-dimensional gas chromatography (GC x GC) measurements of volatile organic compounds in the atmosphere. *Atmos. Chem. Phys.* **2003**, *3*, 665–682.

(7) Park, J. H.; Goldstein, A. H.; Timkovsky, J.; Fares, S.; Weber, R.; Karlik, J.; Holzinger, R. Active atmosphere-ecosystem exchange of the vast majority of detected volatile organic compounds. *Science* **2013**, *341* (6146), 643–647.

(8) Goldstein, A. H.; Galbally, I. E. Known and unexplored organic constituents in the earth's atmosphere. *Environ. Sci. Technol.* **2007**, *41* (5), 1514–1521.

(9) Hunter, J. F.; Day, D. A.; Palm, B. B.; Yatavelli, R. L. N.; Chan, A. H.; Kaser, L.; Cappellin, L.; Hayes, P. L.; Cross, E. S.; Carrasquillo, A. J.; et al. Comprehensive characterization of atmospheric organic carbon at a forested site. *Nat. Geosci.* **2017**, *10* (10), 748–753.

(10) Bryan, A. M.; Cheng, S. J.; Ashworth, K.; Guenther, A. B.; Hardiman, B. S.; Bohrer, G.; Steiner, A. L. Forest-atmosphere BVOC exchange in diverse and structurally complex canopies: 1-D modeling of a mid-successional forest in northern Michigan. *Atmos. Environ.* **2015**, *120*, 217–226.

(11) Palik, B. J.; Pregitzer, K. S. A comparison of pre-settlement and present-day forests on 2 Bigtooth Aspen-dominated landscapes in northern lower Michigan. *Am. Midl. Nat.* **1992**, *127* (2), 327–338.

(12) Carroll, M. A.; Bertman, S. B.; Shepson, P. B. Overview of the Program for Research on Oxidants: PHotochemistry, Emissions, and Transport (PROPHET) summer 1998 measurements intensive. *J. Geophys. Res.* **2001**, *106* (D20), 24275–24288.

(13) Apel, E. C.; Riemer, D. D.; Hills, A.; Baugh, W.; Orlando, J.; Faloona, I.; Tan, D.; Brune, W.; Lamb, B.; Westberg, H. Measurement and interpretation of isoprene fluxes and isoprene, methacrolein, and methyl vinyl ketone mixing ratios at the PROPHET site during the 1998 Intensive. *J. Geophys. Res.* **2002**, *107*, D3 DOI: 10.1029/2000JD000225.

(14) Edwards, G. D.; Martins, D. K.; Starn, T.; Pratt, K.; Shepson, P. B. A disjunct eddy accumulation system for the measurement of BVOC fluxes: instrument characterizations and field deployment. *Atmos. Meas. Tech.* **2012**, *5* (9), 2115–2132.

(15) Edwards, G. D.; Shepson, P. B.; Grossenbacher, J. W.; Wells, J. M.; Patterson, G. E.; Barket, D. J.; Pressley, S.; Karl, T.; Apel, E. Development of an automated cylindrical ion trap mass spectrometer for the determination of atmospheric volatile organic compounds. *Anal. Chem.* **2007**, *79* (13), 5040–5050.

(16) Kim, S.; Guenther, A.; Karl, T.; Greenberg, J. Contributions of primary and secondary biogenic VOC tototal OH reactivity during the CABINEX (Community Atmosphere-Biosphere INteractions Experiments)-09 field campaign. *Atmos. Chem. Phys.* **2011**, *11* (16), 8613–8623.

(17) Mielke, L. H.; Pratt, K. A.; Shepson, P. B.; McLuckey, S. A.; Wisthaler, A.; Hansel, A. Quantitative determination of biogenic volatile organic compounds in the atmosphere using proton-transfer reaction linear ion trap mass spectrometry. *Anal. Chem.* **2010**, *82* (19), 7952–7957.

(18) Pressley, S.; Lamb, B.; Westberg, H.; Flaherty, J.; Chen, J.; Vogel, C. Long-term isoprene flux measurements above a northern hardwood forest. *J. Geophys. Res.* **2005**, *110*, D7 DOI: 10.1029/2004JD005523.

(19) Pressley, S.; Lamb, B.; Westberg, H.; Vogel, C. Relationships among canopy scale energy fluxes and isoprene flux derived from long-term, seasonal eddy covariance measurements over a hardwood forest. *Agr. Forest. Meteorol.* **2006**, *136* (3–4), 188–202.

(20) Turnipseed, A. A.; Pressley, S. N.; Karl, T.; Lamb, B.; Nemitz, E.; Allwine, E.; Cooper, W. A.; Shertz, S.; Guenther, A. B. The use of disjunct eddy sampling methods for the determination of ecosystem level fluxes of trace gases. *Atmos. Chem. Phys.* **2009**, *9* (3), 981−994.

(21) Ortega, J.; Helmig, D.; Guenther, A.; Harley, P.; Pressley, S.; Vogel, C. Flux estimates and OH reaction potential of reactive biogenic volatile organic compounds (BVOCs) from a mixed northern hardwood forest. *Atmos. Environ.* **2007**, *41* (26), 5479−5495.

(22) Kim, S.; Karl, T.; Helmig, D.; Daly, R.; Rasmussen, R.; Guenther, A. Measurement of atmospheric sesquiterpenes by proton transfer reaction-mass spectrometry (PTR-MS). *Atmos. Meas. Tech.* **2009**, *2* (1), 99−112.

(23) Galloway, M. M.; DiGangi, J. P.; Hottle, J. R.; Huisman, A. J.; Mielke, L. H.; Alaghmand, M.; Shepson, P. B.; Weremijewicz, J.; Klavon, H.; McNeal, F. M.; et al. Observations and modeling of formaldehyde at the PROPHET mixed hardwood forest site in 2008. *Atmos. Environ.* **2012**, *49*, 403−410.

(24) Karl, T.; Potosnak, M.; Guenther, A.; Clark, D.; Walker, J.; Herrick, J. D.; Geron, C. Exchange processes of volatile organic compounds above a tropical rain forest: Implications for modeling tropospheric chemistry above dense vegetation. *J. Geophys. Res.* **2004**, *109*, D18 DOI: 10.1029/2004JD004738.

(25) Sumner, A. L.; Shepson, P. B.; Couch, T. L.; Thornberry, T.; Carroll, M. A.; Sillman, S.; Pippin, M.; Bertman, S.; Tan, D.; Faloona, I.; et al. A study of formaldehyde chemistry above a forest canopy. *J. Geophys. Res.* **2001**, *106* (D20), 24387−24405.

(26) Giacopelli, P.; Ford, K.; Espada, C.; Shepson, P. B. Comparison of the measured and simulated isoprene nitrate distributions above a forest canopy. *J. Geophys. Res.* **2005**, *110*, D1 DOI: 10.1029/2004JD005123.

(27) Grossenbacher, J. W.; Couch, T.; Shepson, P. B.; Thornberry, T.; Witmer-Rich, M.; Carroll, M. A.; Faloona, I.; Tan, D.; Brune, W.; Ostling, K. Measurements of isoprene nitrates above a forest canopy. *J. Geophys. Res.* **2001**, *106* (D20), 24429−24438.

(28) Holzinger, R. PTRwid: A new widget tool for processing PTR-TOF-MS data. *Atmos. Meas. Tech.* **2015**, *8* (9), 3903−3922.

(29) Baasandorj, M.; Millet, D. B.; Hu, L.; Mitroo, D.; Williams, B. J. Measuring acetic and formic acid by proton-transfer-reaction mass spectrometry: sensitivity, humidity dependence, and quantifying interferences. *Atmos. Meas. Tech.* **2015**, *8* (3), 1303−1321.

(30) Yuan, B.; Koss, A. R.; Warneke, C.; Coggon, M.; Sekimoto, K.; de Gouw, J. A. Proton-Transfer-Reaction Mass Spectrometry: Applications in atmospheric sciences. *Chem. Rev.* **2017**, *117* (21), 13187−13229.

(31) Yuan, B.; Koss, A.; Warneke, C.; Gilman, J. B.; Lerner, B. M.; Stark, H.; de Gouw, J. A. A high-resolution time-of-flight chemical ionization mass spectrometer utilizing hydronium ions (H_3O^+ ToF-CIMS) for measurements of volatile organic compounds in the atmosphere. *Atmos. Meas. Tech.* **2016**, *9* (6), 2735−2752.

(32) Webb, E. K.; Pearman, G. I.; Leuning, R. Correction of flux measurements for density effects due to heat and water-vapor transfer. *Q. J. R. Meteorol. Soc.* **1980**, *106* (447), 85−100.

(33) de Gouw, J. A.; Goldan, P. D.; Warneke, C.; Kuster, W. C.; Roberts, J. M.; Marchewka, M.; Bertman, S. B.; Pszenny, A. A. P.; Keene, W. C. Validation of proton transfer reaction-mass spectrometry (PTR-MS) measurements of gas-phase organic compounds in the atmosphere during the New England Air Quality Study (NEAQS) in 2002. *J. Geophys. Res.* **2003**, *108*, D21 DOI: 10.1029/2003JD003863.

(34) Hansen, R. F.; Griffith, S. M.; Dusanter, S.; Rickly, P. S.; Stevens, P. S.; Bertman, S. B.; Carroll, M. A.; Erickson, M. H.; Flynn, J. H.; Grossberg, N.; et al. Measurements of total hydroxyl radical reactivity during CABINEX 2009-Part 1: field measurements. *Atmos. Chem. Phys.* **2014**, *14* (6), 2923−2937.

(35) Badol, C.; Borbon, A.; Locoge, N.; Leonardis, T.; Galloo, J. C. An automated monitoring system for VOC ozone precursors in ambient air: development, implementation and data analysis. *Anal. Bioanal. Chem.* **2004**, *378* (7), 1815−1827.

(36) Luke, W. T. Evaluation of a commercial pulsed fluorescence detector for the measurement of low-level SO_2 concentrations during the gas-phase sulfur intercomparison experiment. *J. Geophys. Res.* **1997**, *102* (D13), 16255−16265.

(37) Ridley, B. A.; Grahek, F. E. A small, low flow, high-sensitivity reaction vessel for NO chemiluminescence detectors. *J. Atmos. Ocean Technol.* **1990**, *7* (2), 307−311.

(38) Mauder, M.; Cuntz, M.; Drue, C.; Graf, A.; Rebmann, C.; Schmid, H. P.; Schmidt, M.; Steinbrecher, R. A strategy for quality and uncertainty assessment of long-term eddy-covariance measurements. *Agr. Forest. Meteorol.* **2013**, *169*, 122−135.

(39) Foken, T.; Wichura, B. Tools for quality assessment of surface-based flux measurements. *Agr. Forest. Meteorol.* **1996**, *78* (1−2), 83−105.

(40) Horst, T. W. A simple formula for attenuation of eddy fluxes measured with first-order-response scalar sensors. *Bound.-Lay. Meteorol.* **1997**, *82* (2), 219−233.

(41) Lin, S.-J.; Rood, R. B. Multidimensional flux form semi-Lagrangian transport schemes. *Mon. Weather Rev.* **1996**, *124*, 2046−2070.

(42) Wu, S. L.; Mickley, L. J.; Jacob, D. J.; Logan, J. A.; Yantosca, R. M.; Rind, D. Why are there large differences between models in global budgets of tropospheric ozone? *J. Geophys. Res.* **2007**, *112* (D5), D05302.

(43) Lin, J.-T.; McElroy, M. Impacts of boundary layer mixing on pollutant vertical profiles in the lower troposphere: Implications to satellite remote sensing. *Atmos. Environ.* **2010**, *44*, 1726−1739.

(44) Amos, H. M.; Jacob, D. J.; Holmes, C. D.; Fisher, J. A.; Wang, Q.; Yantosca, R. M.; Corbitt, E. S.; Galarneau, E.; Rutter, A. P.; Gustin, M. S.; et al. Gas-particle partitioning of atmospheric Hg(II) and its effect on global mercury deposition. *Atmos. Chem. Phys.* **2012**, *12*, 591−603.

(45) Wang, Y. H.; Jacob, D. J.; Logan, J. A. Global simulation of tropospheric O_3-NO_x-hydrocarbon chemistry: 1. Model formulation. *J. Geophys. Res.* **1998**, *103* (D9), 10713−10725.

(46) Kim, P. S.; Jacob, D. J.; Fisher, J. A.; Travis, K.; Yu, K.; Zhu, L.; Yantosca, R. M.; Sulprizio, M. P.; Jimenez, J. L.; Campuzano-Jost, P.; et al. Sources, seasonality, and trends of Southeast US aerosol: An integrated analysis of surface, aircraft, and satellite observations with the GEOS-Chem chemical transport model. *Atmos. Chem. Phys.* **2015**, *15*, 10411−10433.

(47) Philip, S.; Martin, R. V.; Keller, C. A. Sensitivity of chemistry-transport model simulations to the duration of chemical and transport operators: a case study with GEOS-Chem v10−01. *Geosci. Model Dev.* **2016**, *9* (5), 1683−1695.

(48) Bian, H.; Prather, M. J. Fast-J2: Accurate simulation of stratospheric photolysis in global chemical models. *J. Atmos. Chem.* **2002**, *41*, 281−296.

(49) Eastham, S. D.; Weisenstein, D. K.; Barrett, S. R. H. Development and evaluation of the unified tropospheric-stratospheric chemistry extension (UCX) for the global chemistry-transport model GEOS-Chem. *Atmos. Environ.* **2014**, *89*, 52−63.

(50) Mao, J.; Paulot, F.; Jacob, D. J.; Cohen, R. C.; Crounse, J. D.; Wennberg, P. O.; Keller, C. A.; Hudman, R. C.; Barkley, M. P.; Horowitz, L. W. Ozone and organic nitrates over the eastern United States: Sensitivity to isoprene chemistry. *J. Geophys. Res.* **2013**, *118*, 11256−11268.

(51) Millet, D. B.; Baasandorj, M.; Farmer, D. K.; Thornton, J. A.; Baumann, K.; Brophy, P.; Chaliyakunnel, S.; Gouw, J. A. d.; Graus, M.; Hu, L.; et al. A large and ubiquitous source of atmospheric formic acid. *Atmos. Chem. Phys.* **2015**, *15*, 6283−6304.

(52) Paulot, F.; Wunch, D.; Crounse, J. D.; Toon, G. C.; Millet, D. B.; DeCarlo, P. F.; Vigouroux, C.; Deutscher, N. M.; Abad, G. G.; Notholt, J.; et al. Importance of secondary sources in the atmospheric budgets of formic and acetic acids. *Atmos. Chem. Phys.* **2011**, *11*, 1989−2013.

(53) Fischer, E. V.; Jacob, D. J.; Yantosca, R. M.; Sulprizio, M. P.; Millet, D. B.; Mao, J.; Paulot, F.; Singh, H. B.; Roiger, A.; Ries, L.;

et al. Atmospheric peroxyacetyl nitrate (PAN): a global budget and source attribution. *Atmos. Chem. Phys.* **2014**, *14* (5), 2679−2698.

(54) Fu, T. M.; Jacob, D. J.; Wittrock, F.; Burrows, J. P.; Vrekoussis, M.; Henze, D. K. Global budgets of atmospheric glyoxal and methylglyoxal, and implications for formation of secondary organic aerosols. *J. Geophys. Res.* **2008**, *113*, D15303.

(55) Hu, L.; Millet, D. B.; Baasandorj, M.; Griffis, T. J.; Travis, K. R.; Tessum, C. W.; Marshall, J. D.; Reinhart, W. F.; Mikoviny, T.; Müller, M.; et al. Emissions of C_6-C_8 aromatic compounds in the United States: Constraints from tall tower and aircraft measurements. *J. Geophys. Res.* **2015**, *120*, 826−842.

(56) Millet, D. B.; Apel, E.; Henze, D. K.; Hill, J.; Marshall, J. D.; Singh, H. B.; Tessum, C. W. Natural and anthropogenic ethanol sources in North America and potential atmospheric impacts of ethanol fuel use. *Environ. Sci. Technol.* **2012**, *46* (15), 8484−8492.

(57) Millet, D. B.; Guenther, A.; Siegel, D. A.; Nelson, N. B.; Singh, H. B.; de Gouw, J. A.; Warneke, C.; Williams, J.; Eerdekens, G.; Sinha, V.; et al. Global atmospheric budget of acetaldehyde: 3D model analysis and constraints from in-situ and satellite observations. *Atmos. Chem. Phys.* **2010**, *10*, 3405−3425.

(58) Millet, D. B.; Jacob, D. J.; Custer, T. G.; de Gouw, J. A.; Goldstein, A. H.; Karl, T.; Singh, H. B.; Sive, B. C.; Talbot, R. W.; Warneke, C.; et al. New constraints on terrestrial and oceanic sources of atmospheric methanol. *Atmos. Chem. Phys.* **2008**, *8*, 6887−6905.

(59) Wells, K. C.; Millet, D. B.; Cady-Pereira, K. E.; Shephard, M. W.; Henze, D. K.; Bousserez, N.; Apel, E. C.; Gouw, J. A. d.; Warneke, C.; Singh, H. B. Quantifying global terrestrial methanol emissions using observations from the TES satellite sensor. *Atmos. Chem. Phys.* **2014**, *14*, 2555−2570.

(60) Keller, C. A.; Long, M. S.; Yantosca, R. M.; Da Silva, A. M.; Pawson, S.; Jacob, D. J. HEMCO v1.0: a versatile, ESMF-compliant component for calculating emissions in atmospheric models. *Geosci. Model Dev.* **2014**, *7* (4), 1409−1417.

(61) Hu, L.; Millet, D. B.; Baasandorj, M.; Griffis, T. J.; Turner, P.; Helmig, D.; Curtis, A. J.; Hueber, J. Isoprene emissions and impacts over an ecological transition region in the US Upper Midwest inferred from tall tower measurements. *J. Geophys. Res.* **2015**, *120*, 3553−3571.

(62) Myneni, R. B.; Yang, W.; Nemani, R. R.; Huete, A. R.; Dickinson, R. E.; Knyazikhin, Y.; Didan, K.; Fu, R.; Negron Juarez, R. I.; Saatchi, S. S.; et al. Large seasonal swings in leaf area of Amazon rainforests. *Proc. Natl. Acad. Sci. U. S. A.* **2007**, *104* (12), 4820−4823.

(63) Oleson, K. W.; Lawrence, D. M.; Bonan, G. B.; Flanner, M. G.; Kluzek, E.; Lawrence, P. J.; Levis, S.; Swenson, S. C.; Thornton, P. E.; Dai, A.; et al. *Technical Description of version 4.0 of the Community Land Model (CLM): Technical Note NCAR/TN-478+STR*; National Center for Atmospheric Research: Boulder, CO, 2010; p 173.

(64) Guenther, A.; Karl, T.; Harley, P.; Wiedinmyer, C.; Palmer, P. I.; Geron, C. Estimates of global terrestrial isoprene emissions using MEGAN (Model of Emissions of Gases and Aerosols from Nature). *Atmos. Chem. Phys.* **2006**, *6*, 3181−3210.

(65) Lamarque, J. F.; Bond, T. C.; Eyring, V.; Granier, C.; Heil, A.; Klimont, Z.; Lee, D.; Liousse, C.; Mieville, A.; Owen, B.; et al. Historical (1850−2000) gridded anthropogenic and biomass burning emissions of reactive gases and aerosols: methodology and application. *Atmos. Chem. Phys.* **2010**, *10* (15), 7017−7039.

(66) Riahi, K.; Rao, S.; Krey, V.; Cho, C. H.; Chirkov, V.; Fischer, G.; Kindermann, G.; Nakicenovic, N.; Rafaj, P. RCP 8.5-A scenario of comparatively high greenhouse gas emissions. *Clim. Change* **2011**, *109* (1−2), 33−57.

(67) van Vuuren, D. P.; Edmonds, J.; Kainuma, M.; Riahi, K.; Thomson, A.; Hibbard, K.; Hurtt, G. C.; Kram, T.; Krey, V.; Lamarque, J. F.; et al. The representative concentration pathways: an overview. *Clim. Change* **2011**, *109* (1−2), 5−31.

(68) European Commission. *Emission Database for Global Atmospheric Research (EDGAR), release version 4.2*; Joint Research Centre: 2011; http://edgar.jrc.ec.europa.eu, accessed on 06/17/2015.

(69) Hudman, R. C.; Moore, N. E.; Mebust, A. K.; Martin, R. V.; Russell, A. R.; Valin, L. C.; Cohen, R. C. Steps towards a mechanistic model of global soil nitric oxide emissions: implementation and space based-constraints. *Atmos. Chem. Phys.* **2012**, *12* (16), 7779−7795.

(70) EPA. 2011 National Emissions Inventory. https://www.epa.gov/air-emissions-inventories/2011-national-emission-inventory-nei-report, accessed on 06/17/2015, 2015.

(71) Travis, K. R.; Jacob, D. J.; Fisher, J. A.; Kim, P. S.; Marais, E. A.; Zhu, L.; Yu, K.; Miller, C. C.; Yantosca, R. M.; Sulprizio, M. P.; et al. Why do models overestimate surface ozone in the Southeast United States? *Atmos. Chem. Phys.* **2016**, *16* (21), 13561−13577.

(72) Fischer, E. V.; Jacob, D. J.; Millet, D. B.; Yantosca, R. M.; Mao, J. The role of the ocean in the global atmospheric budget of acetone. *Geophys. Res. Lett.* **2012**, *39*, L01807.

(73) Giglio, L.; Randerson, J. T.; van der Werf, G. R. Analysis of daily, monthly, and annual burned area using the fourth-generation global fire emissions database (GFED4). *J. Geophys. Res.: Biogeosci.* **2013**, *118* (1), 317−328.

(74) van der Werf, G. R.; Randerson, J. T.; Giglio, L.; Collatz, G. J.; Mu, M.; Kasibhatla, P. S.; Morton, D. C.; DeFries, R. S.; Jin, Y.; van Leeuwen, T. T. Global fire emissions and the contribution of deforestation, savanna, forest, agricultural, and peat fires (1997−2009). *Atmos. Chem. Phys.* **2010**, *10*, 11707−11735.

(75) Xiao, Y. P.; Logan, J. A.; Jacob, D. J.; Hudman, R. C.; Yantosca, R.; Blake, D. R. Global budget of ethane and regional constraints on US sources. *J. Geophys. Res.* **2008**, *113*, D21306.

(76) Stettler, M. E. J.; Eastham, S.; Barrett, S. R. H. Air quality and public health impacts of UK airports. Part I: Emissions. *Atmos. Environ.* **2011**, *45* (31), 5415−5424.

(77) Holmes, C. D.; Prather, M. J.; Vinken, G. C. M. The climate impact of ship NO_x emissions: an improved estimate accounting for plume chemistry. *Atmos. Chem. Phys.* **2014**, *14* (13), 6801−6812.

(78) Murray, L. T.; Jacob, D. J.; Logan, J. A.; Hudman, R. C.; Koshak, W. J. Optimized regional and interannual variability of lightning in a global chemical transport model constrained by LIS/OTD satellite data. *J. Geophys. Res.* **2012**, *117*, D20307.

(79) Kaser, L.; Karl, T.; Guenther, A.; Graus, M.; Schnitzhofer, R.; Turnipseed, A.; Fischer, L.; Harley, P.; Madronich, M.; Gochis, D.; et al. Undisturbed and disturbed above canopy ponderosa pine emissions: PTR-TOF-MS measurements and MEGAN 2.1 model results. *Atmos. Chem. Phys.* **2013**, *13* (23), 11935−11947.

(80) Atkinson, R.; Baulch, D. L.; Cox, R. A.; Crowley, J. N.; Hampson, R. F.; Hynes, R. G.; Jenkin, M. E.; Rossi, M. J.; Troe, J. Evaluated kinetic and photochemical data for atmospheric chemistry: Volume II - gas phase reactions of organic species. *Atmos. Chem. Phys.* **2006**, *6* (11), 3625−4055.

(81) Donahue, N. M.; Chuang, W.; Epstein, S. A.; Kroll, J. H.; Worsnop, D. R.; Robinson, A. L.; Adams, P. J.; Pandis, S. N. Why do organic aerosols exist? Understanding aerosol lifetimes using the two-dimensional volatility basis set. *Environ. Chem.* **2013**, *10* (3), 151−157.

(82) Di Carlo, P.; Brune, W. H.; Martinez, M.; Harder, H.; Lesher, R.; Ren, X. R.; Thornberry, T.; Carroll, M. A.; Young, V.; Shepson, P. B.; et al. Missing OH reactivity in a forest: Evidence for unknown reactive biogenic VOCs. *Science* **2004**, *304* (5671), 722−725.